JACS
JOURNAL OF THE AMERICAN CHEMICAL SOCIETY
Article
pubs.acs.org/JACS

Unprecedented Topological Complexity in a Metal–Organic Framework Constructed from Simple Building Units

A. Ken Inge,*[,†,‡] Milan Köppen,[†] Jie Su,[‡] Mark Feyand,[†] Hongyi Xu,[‡] Xiaodong Zou,[‡] Michael O'Keeffe,*[,§] and Norbert Stock*[,†]

[†]Institut für Anorganische Chemie, Christian-Albrechts-Universität zu Kiel, Max-Eyth-Str. 2, 24118 Kiel, Germany

[‡]Berzelii Center EXSELENT on Porous Materials and Department of Materials and Environmental Chemistry, Stockholm University, Stockholm S-106 91, Sweden

[§]School of Molecular Sciences, Arizona State University, Tempe, Arizona 85287-1604, United States

Supporting Information

ABSTRACT: A bismuth-based metal–organic framework (MOF), $[Bi(BTC)(H_2O)]\cdot 2H_2O\cdot MeOH$ denoted CAU-17, was synthesized and found to have an exceptionally complicated structure with helical Bi–O rods cross-linked by 1,3,5-benzenetricarboxylate (BTC^{3-}) ligands. Five crystallographically independent 1D channels including two hexagonal channels, two rectangular channels, and one triangular channel have accessible diameters of 9.6, 9.6, 3.6, 3.6, and 3.4 Å, respectively. The structure is further complicated by twinning. Rod-incorporated MOF structures typically have underlying nets with only one unique node and three or four unique edges. In contrast, topological analysis of CAU-17 revealed unprecedented complexity for a MOF structure with 54 unique nodes and 135 edges. The complexity originates from the rod packing and the rods themselves, which are related to aperiodic helices.

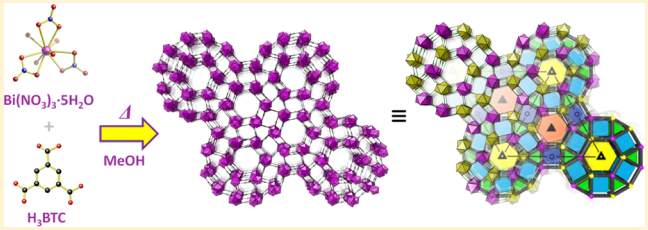

INTRODUCTION

Research in various fields of chemistry is largely focused on the determination and description of the arrangement of atoms. For chemical compounds with more complex structures an improved understanding of the connections between atomic or molecular building units can be achieved by deconstructing their structures into a simpler net. Nodes in a net can represent certain atoms, ions, molecules, or larger secondary building units (SBUs) such as clusters, while the connections between these building units are represented as linear links (edges). A measure of the complexity of a net is its *transitivity p q*, which indicates that there are *p* different (i.e., unrelated by the intrinsic symmetry of the net) kinds of nodes and *q* kinds of links. The mineral low-tridymite, a polymorph of SiO_2, has a complex crystal structure with 80 silicon atoms and 160 oxygen atoms in the asymmetric unit. Topological analysis, however, reveals that the underlying net is in fact very simple with just one kind of node and two kinds of edges (transitivity 1 2).[1]

Topological analysis is particularly useful in simplifying, understanding, comparing, and predicting the structures of crystalline open-framework materials where the arrangement of atoms governs the pore size, shape, and volume. Metal–organic frameworks (MOFs)[2−4] are a class of inorganic–organic framework materials[5] constructed of strongly bonded cations and polytopic organic linkers assembled into open frameworks. In such materials individual metal cations, or an assembly of multiple cations in SBUs, are linked together by polytopic organic molecules such as polycarboxylates. Due to their diverse crystal structures and chemical compositions MOFs have been intensely studied for potential applications regarding gas storage, heterogeneous catalysis, separation, drug delivery, and as sensors.[3,6−8]

The deconstruction of MOF structures into their underlying nets starts by identifying the SBUs. These in turn are defined by the pattern of points of extension that mark the interface between the inorganic and organic components of the structure. In carboxylate-based MOFs these are generally the carbon atoms of the carboxylate group.[2] For MOFs with finite SBUs, the structure is simplified by taking the center of the SBU as a node. Linkers may also be represented by nodes if they are not ditopic. Most MOFs have underlying nets of minimal transitivity[9]—the fewest number of unique nodes and edges compatible with the local structure—including iconic MOFs such as MOF-5[10] and HKUST-1[11] with transitivity 1 1 and 2 1, respectively. Examples of complex MOF nets containing finite SBUs are those of MIL-100[12,13] and ZIF-100.[14] The underlying net of ZIF-100 has 10 topologically distinct nodes and 22 links (perhaps the largest for any MOF comprised of finite SBUs). MOFs constructed of finite SBUs such as clusters or individual polyhedra can have interpenetrated networks, resulting in reduced accessibility of the pores and reduced pore volume.[15−17]

Received: November 30, 2015
Published: January 21, 2016

DOI: 10.1021/jacs.5b12484
J. Am. Chem. Soc. 2016, 138, 1970−1976

One strategy to obtain porous materials and avoid the issue of interpenetration is to construct frameworks from infinite SBUs such as rods.[18] However, for MOFs with infinitely long SBUs, the points of extension themselves should be selected as the nodes. This has been established in a previous extensive study on rod-based MOFs[18] and is a systematic method used in order to obtain an underlying net in which chemical significance and information regarding the rods is not lost. If one were to select the metal cations in a rod-based MOF as nodes, then all sense of a rod-based structure would be lost, resulting in a net that no longer resembles the original crystal structure. For consistency, the branch points of polytopic linkers in rod MOFs are represented by a polygon or polyhedron. In the case of a tritopic linker such as 1,3,5-benzenetricarboxylate (BTC^{3-}), they are represented by a triangle (Figure 1).[19] For the nets of many common rod-based

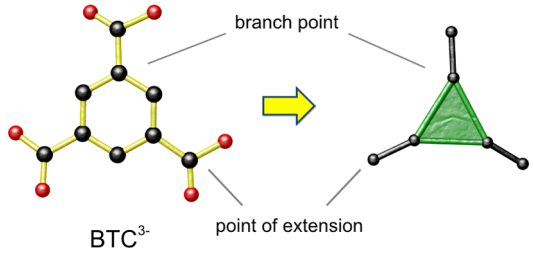

Figure 1. Deconstruction of the BTC^{3-} linker in CAU-17 into nodes and edges. The carboxylate carbon atoms, representing the points of extension, and the branch points on the benzene ring are selected as nodes in the BTC^{3-} linker.

MOFs the transitivity is 1 3 or 1 4 typically.[20] This is in accord with the principle of minimal transitivity which states that the transitivity will be the smallest possible compatible with the local structure of the components.[9] Recently a rod-based MOF reported by Song et al., $[In(OH)L]_5(NO_3)_5{\cdot}33H_2O{\cdot}14DMF$ where L = 1,3-bis(4-carboxyphenyl)imidazolium,[21] was found on topological analysis to have an underlying net of exceptional complexity—transitivity 10 25 (Figure 2). This was in fact explained to be minimal transitivity consistent with local 5-fold helical symmetry of the rod.[22]

Infinitely large inorganic SBUs, such as rods and layers, are common among Bi^{3+}-containing inorganic−organic framework materials. However, relatively few MOFs exhibiting permanent porosity have been constructed using Bi^{3+} cations. Bismuth is considered nontoxic, and its complexes are of interest in medical applications regarding their antitumor and antimicrobial activities as well as treatment for dyspepsia.[23−26] Hence Bi-MOFs are of interest as potential drug delivery carriers. Although many bismuth-containing inorganic−organic framework materials have been reported,[27−31] nearly all are dense nonporous materials, and it remains a challenge to construct open-framework MOFs from bismuth cations. The tendency of Bi^{3+} to form layered or dense frameworks is attributed to the high coordination number and flexible coordination geometry of the cation.[19] Only two open Bi-MOF structures exhibiting permanent porosity have been published as far as we know including CAU-7 ([Bi(BTB)], where BTB = 1,3,5-benzenetrisbenzoate)[32] and NOTT-220 ($[Bi_2(L)_{1.5}(H_2O)_2]{\cdot}3.5DMF{\cdot}3H_2O$, where L = biphenyl-3,3′,5,5′-tetracarboxylate).[33] We now report a rod-based Bi-MOF with underlying net of transitivity 54 135—a net of unprecedented complexity among MOF structures. The intricacy of the net arises in part from the use of a tritopic linker as supposed to a ditopic linker, complexity of the rods themselves, and the presence of three distinct independent helical rods in the framework.

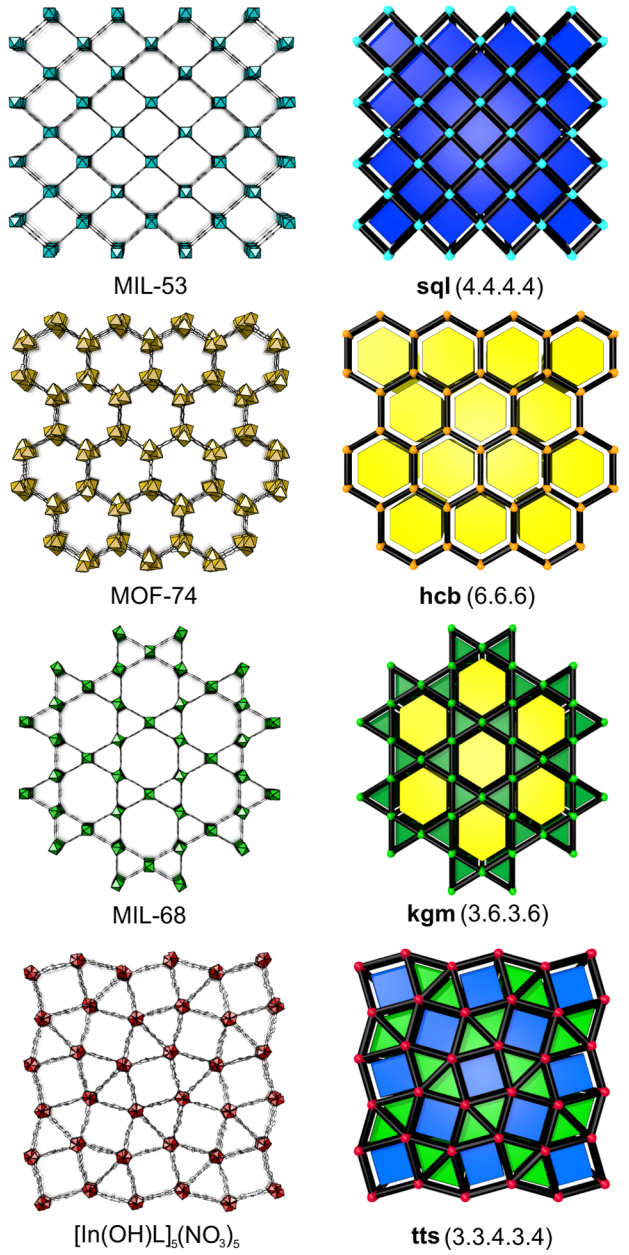

Figure 2. Select rod-based MOFs and 2-periodic nets describing the packing of rods. Included are MIL-53 with rods falling on a square net (**sql**), MOF-74 with a honeycomb net (**hcb**), MIL-68 with the kagome net (**kgm**), and an indium-MOF with rods on the **tts** net of which the 3-periodic net has the highest transitivity among MOFs until now. Vertex symbols are shown below the three letter symbols of each 2-periodic net.

RESULTS AND DISCUSSION

Crystal Structure Description. CAU-17 exhibits an intricate 3D extended crystalline open-framework structure (Figure 3a). Structure determination and refinement details are provided in the methods section and in further details in the Supporting Information. Although a large number of framework species are present in the asymmetric unit (nine Bi^{3+}, nine BTC^{3-}, and nine coordinated water molecules), the local

DOI: 10.1021/jacs.5b12484
J. Am. Chem. Soc. 2016, 138, 1970−1976

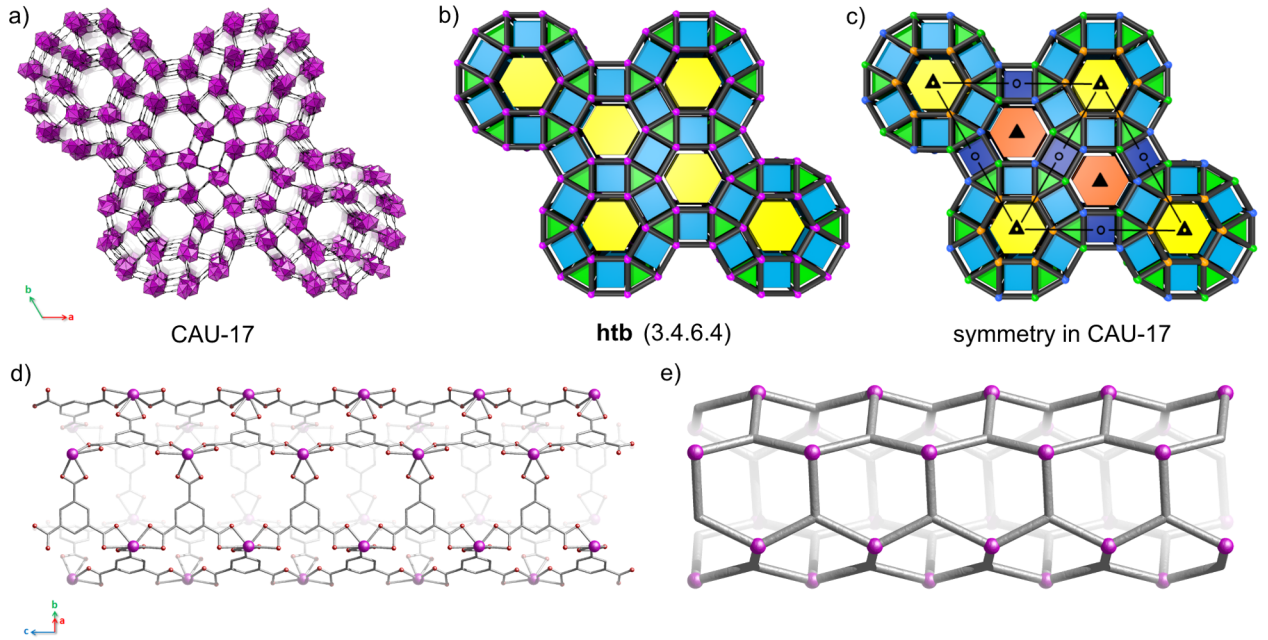

Figure 3. (a) Crystal structure of CAU-17. Bismuth−oxygen polyhedra are colored purple. (b) The rods fall on the 2-periodic **htb** net which has one type of node (purple), one type of triangle (green), one type of square (light blue), and one type of hexagon (yellow). (c) The **htb** net is overlaid with symmetry elements found in CAU-17 (space group $P\bar{3}$) and the unit cell edges. Unlike the standard **htb** net, CAU-17 has three symmetry-independent rods (orange, green, and blue nodes), two hexagonal channels (orange and yellow hexagons), and two independent rectangular channels (light and dark blue rectangles) and one type of triangular channel (green triangle). (d) The inner wall of one of the hexagonal channels of CAU-17 viewed perpendicular to the *c*-axis. (e) The connectivity within the inner walls of the hexagonal channels resembles achiral carbon nanotubes of the armchair type.

environments around each of these species do not significantly differ apart from small distortions in bond lengths and angles; i.e., all the Bi^{3+} as well as all BTC^{3-} have relatively similar coordination environments (Figure S1, Figure S2, and Table S2). Each Bi^{3+} is coordinated by nine oxygen atoms. Eight of these oxygen atoms belong to carboxylate groups of the BTC^{3-}. The ninth coordinating oxygen atom is a terminal water molecule. Each Bi^{3+} shares four oxygen atoms with two neighboring Bi^{3+} resulting in helical rods (approximately 3_1 and 3_2 symmetry) along the *c*-axis. These extended rods each consist of three symmetry-independent Bi^{3+}. Each rod is interconnected to four other rods via bridging BTC^{3-}.

Packing of Rods in the 2-Periodic Net and Description of Channels. The rod packing itself in CAU-17 is highly unusual. Generally structures with parallel rods have the axes on a simple square,[34,35] hexagonal,[18,32] or kagome net[36] (Figure 2). The vertex symbol of these 2-periodic nets indicates the type of polygons and the order in which they meet at a vertex. For example in a square lattice (**sql** net) the net comprises only one type of polygon: squares (4). Around each vertex are four squares, hence the vertex symbol is 4.4.4.4 or more commonly 4^4. In the kagome net (**kgm** net) four polygons meet at each vertex, and the vertex symbol is 3.6.3.6. The recently reported structure of Song et al.[21] is a rare exception with rod axes falling on a 3.3.4.3.4 or 3^2.4.3.4 (**tts**) net, but this was explained as a consequence of local pentagonal symmetry. In the structure presented here the rod axes are on a 3.4.6.4 net (Figure 3b), also known as the hexagonal tungsten bronze (**htb**) net; as far as we know, the first such. However, the **htb** net represents a 2D perspective of the *ab*-plane assuming all rods are symmetry related, which is not the case in CAU-17. Instead there are three crystallographically independent rods in CAU-17 (Figure 3c).

The rods in CAU-17 form the edges of the five crystallographically independent channels, including two hexagonal channels, two rectangular channels, and one triangular channel, with accessible diameters of 9.6, 9.6, 3.6, 3.6, and 3.4 Å, respectively, as calculated accounting for the van der Waals radii of carbon and oxygen atoms of the pore walls. All channels are aligned parallel to the *c*-axis. The hexagonal channels are not interconnected to any of the other channels and are circumscribed by a double wall of BTC^{3-} ligands. The windows in these double walls are blocked by the coordinated water molecules, leaving only a void of 0.9 Å in diameter. The inner walls of the hexagonal channels alone (Figure 3d) are topologically similar to achiral carbon nanotubes (CNTs) of the armchair type[37] (Figure 3e). In contrast the sides of the triangular channels are composed of a single wall. The rectangular channels have two single walls on opposite sides and two double walls (Figure S3). The double walls are stabilized by $\pi-\pi$ stacking of BTC^{3-} (3.78−3.98 Å between the centers of the benzene rings and slippage angles 15−17°).[38]

Deconstruction of the Crystal Structure into Its Underlying 3-Periodic Net. As aforementioned the points of extension and branch points in the linker should be chosen as the nodes of the underlying 3-periodic net (Figure 1). Around each helical bismuth-carboxylate rod (Figure 4a) the pattern of just the points of extension (carboxylate C atoms, Figure 4b) is that of a rod of face-sharing octahedra (Figure 4c). Rods of octahedra sharing opposite faces are commonly found in other rod-based MOFs,[19] and each node on such rod has six neighbors. Within the present rod, each octahedron shares two of its faces with a common vertex with neighboring octahedra, and there are three topologically distinct kinds of nodes that are 4-, 6-, and 8-coordinated. Such a helix made of regular octahedra was described by Lidin and Andersson[39] who showed

DOI: 10.1021/jacs.5b12484
J. Am. Chem. Soc. 2016, 138, 1970−1976

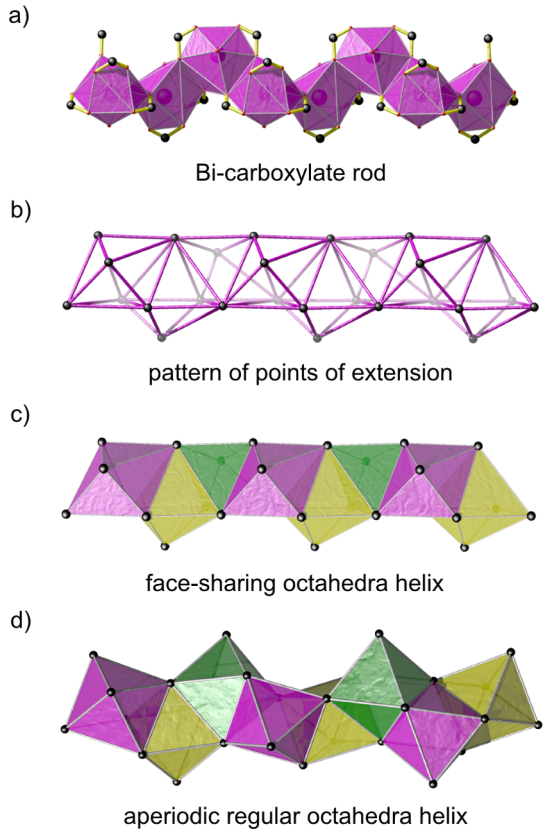

Figure 4. Deconstruction of bismuth-carboxylate rods in CAU-17 into the pattern of points of extension. (a) A bismuth-carboxylate helical rod with carboxylate carbon atoms shown in black. (b) The nodes representing the carboxylate carbon atoms are connected forming hollow face-sharing distorted octahedra. (c) The distorted octahedra are colored purple, yellow, and green to distinguish between neighbors. (d) Face-sharing of regular octahedra in the same manner results in an aperiodic helix.

that it was aperiodic (Figure 4d), so the octahedra must be distorted if the rod is to be realized in a periodic structure as seen for CAU-17.

The rods of distorted face-sharing octahedra are cross-linked to one another via the nodes representing the branch points of the linker, illustrated as green triangles. Rods are single linked forming single walls of the triangular channels (Figure 5a,b) or double linked forming the double walls of the hexagonal channels (Figure 5c,d).

The entire 3-periodic net is illustrated in Figure 6a with the 2-periodic rod packing representation shown in Figure 6b, indicating the handedness of the rods and the five unique channels.

The 3-periodic net of CAU-17 has an unprecedented number of nodes among MOFs, which are calculated as follows:

1. For each Bi^{3+} ion there are three carboxylate nodes to achieve charge balance which represent the points of extension (3 carboxylate nodes).
2. Each rod consists of three independent Bi^{3+} ($3 \times 3 = 9$ carboxylate nodes).
3. There are three independent rods in the crystal structure ($3 \times 3 \times 3 = 27$ carboxylate nodes).
4. Each of the 27 carboxylate nodes has a corresponding node in the benzene ring representing the 27 branch points ($3 \times 3 \times 3 \times 2 = 54$ total nodes).

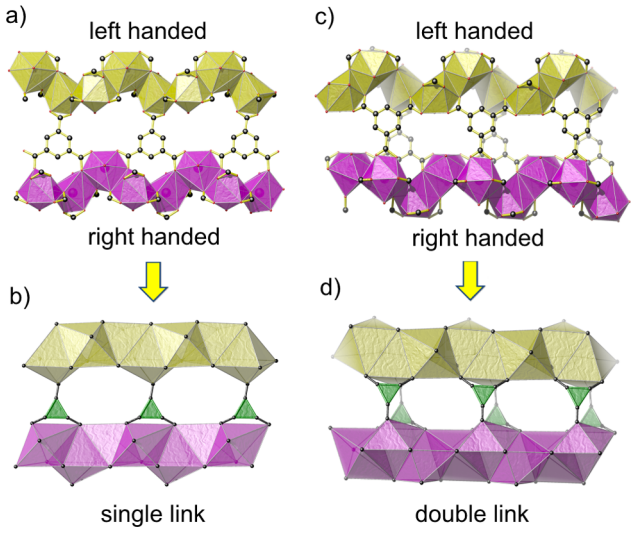

Figure 5. Deconstruction of CAU-17 into its underlying 3-periodic net. (a) Two helical rods connected by one set of BTC^{3-} linkers are shown as found in the triangular channels. Right-handed and left-handed helices are colored purple and yellow, respectively, here and henceforth. (b) The topological representation of two rods single linked by BTC^{3-}. (c) Two helical rods double linked by BTC^{3-} are shown such as those found around the hexagonal channels. (d) The topological representation of two rods double linked by BTC^{3-}.

5. 135 edges connect the 54 nodes to achieve transitivity of 54 135.

Submitting the net defined by these 54 nodes to Systre[40] confirmed that all these nodes are topologically distinct and that the intrinsic symmetry was that of the crystal, $P\bar{3}$ (see Supporting Information). This is a quite remarkable result. The net containing 54 nodes is far from minimal transitivity as a net of minimal transitivity based on a tritopic linker would have just two nodes. The individual rods in the structure are all topologically identical with just three kinds of nodes that are 5-, 7-, and 9-coordinated (each of the 4-, 6-, and 8-coordinated nodes in the rod gains one link through the connection of the rods). Likewise all the linkers individually are identical, but when assembled there are three distinct rods each with nine kinds of nodes and nine kinds of linkers. It is emphasized that these distinctions are topological—there is no possible higher-symmetry embedding of the net. The lack of symmetry operations that relate the large number of nodes in the net with one another explains the large number of Bi^{3+} cations and BTC^{3-} anions in the asymmetric unit.

Limitations in the Rod Packing. Limitations in the ways the particular rods of CAU-17 connect to one another in the 2-periodic **htb** net have been observed. There are an even number of left (L) and right (R) handed rods in CAU-17 but only one crystallographically independent triangular channel in CAU-17 (Figure 6b). The handedness of the three rods forming the edges of the triangular channels are either RRL or LLR, which are related by inversion symmetry. The configurations RRR or LLL are less favorable (Figure S5) as the height of the BTC^{3-} cross-links between rods along the *c*-axis would be severely misaligned. This misalignment would result in either severe distortion of the rods or BTC^{3-} anions would have to be missing, and charge balance of the Bi^{3+} must be achieved by other means.

On the other hand there are two crystallographically independent hexagonal channels where one is centered along

DOI: 10.1021/jacs.5b12484
J. Am. Chem. Soc. 2016, 138, 1970−1976

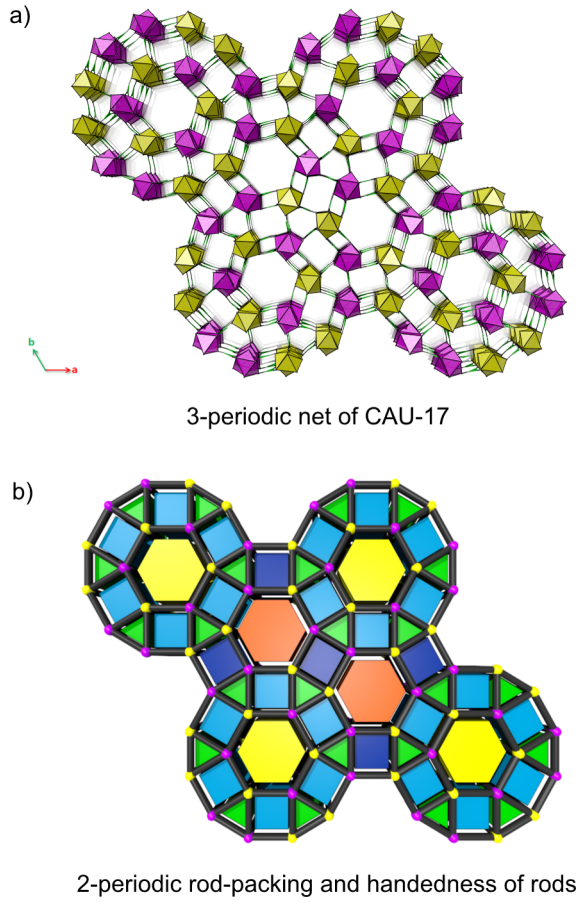

Figure 6. Deconstruction of CAU-17 into its underlying net. (a) The 3-periodic net of CAU-17 along [001]. (b) The **htb** net with nodes colored in accordance to the handedness of the helices in CAU-17. Symmetry equivalent channels, represented by polygons, are colored similarly.

a 3-fold rotation axis and the other is centered along a $\bar{3}$-axis. Despite there being two crystallographically independent hexagonal channels, these two channels are similar in terms of their local environments and local symmetry—one can be generated through rotation of the other by 60° and translation, such as $(1/3x, 2/3y,$ and $0z)$ along the unit cell. The reason why the channels are indeed crystallographically independent is due to the different arrangement of adjacent rectangular channels. Only one of the two rectangular channels has inversion symmetry and has the configuration RRLL, whereas the other rectangular channel follows the configuration RLRL and lacks inversion symmetry. Out of the two hexagonal channels, the one centered along the $\bar{3}$-axis is surrounded by six rectangular channels of the configuration RLRL, while the other hexagonal channel centered around the 3-fold axis has alternating RLRL and RRLL rectangular channels (Figure S4).

Adjacent rods of the hexagonal channels must have opposite handedness (RL) in order to have double links between neighboring rods. If two adjacent rods were to have the same handedness (RR or LL), it would lead to a mismatch in the height of one of the two sets of BTC^{3-} linkers in the double wall (Figure S5). The absence of RR/LL connections in the hexagonal channels and the absence of RRR/LLL triangular channels prevent the structure from crystallizing in a smaller trigonal unit cell (i.e., a structure with the **htb** net and only one unique rod). In this smaller hypothetical unit cell (Figure S6), only one independent hexagonal channel would exist in the structure. However, if all adjacent rods along the hexagonal channels have opposite handedness then all triangular channels would exclusively have the configurations RRR or LLL. Therefore, the crystalline structure must have at least two crystallographically independent hexagonal channels to follow these two cross-linking conditions.

Twinning. Single-crystal X-ray diffraction data collected on all seven different examined crystals of CAU-17 indicated merohedral twinning of equal components, with a twin operation corresponding to a 2-fold rotation along the *c*-axis (Figure 7a and Figure 7b). The RLRL rectangular channels

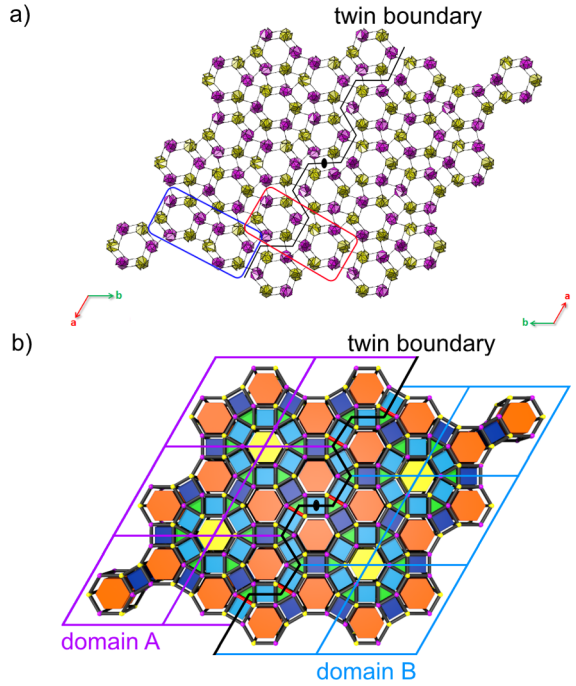

Figure 7. Twinning in CAU-17. Right-handed and left-handed rods are colored purple and yellow, respectively. (a) A model of two domains related by 2-fold symmetry is illustrated with the twin boundary shown by black lines. A 2-fold axis on the twin boundary is shown as a filled ellipse at the center of the figure. An ordered pair of hexagonal channels in blue is compared to a pair across the twin boundary in red. (b) The simplified 2-periodic model with rods represented as nodes and the unit cell edges of the two domains outlined in purple and blue. Edges shown in red across the twin boundary indicate strained links due to a shift of 0.6 Å in the height of BTC^{3-} linkers along the *c*-axis.

have pseudo-2-fold symmetry if their surroundings are neglected (Figure S3d). Hence it is presumed the 2-fold twin operation lies centered in RLRL rectangular channels. This form of twinning would result in the handedness of some of the rods to be reversed across the twin boundary. For example a right-handed rod that normally connects to a right-handed rod in an ordered domain of the crystal structure may instead connect to a left-handed rod across the twin boundary forming a defect. As a result some RRLL rectangular channels (Figure 8a) are converted into RLRL channels (Figure 8b).

In the illustrated twin model, one out of four BTC^{3-} ligands along the twin boundary is slightly shifted along the *c*-axis (0.6 Å) as indicated by a red edge in Figure 7b. The typical Bi−O bond range is 2.2−3.0 Å in bismuth-carboxylate inorganic−organic framework materials. However, in these shifted BTC^{3-}

DOI: 10.1021/jacs.5b12484
J. Am. Chem. Soc. 2016, 138, 1970−1976

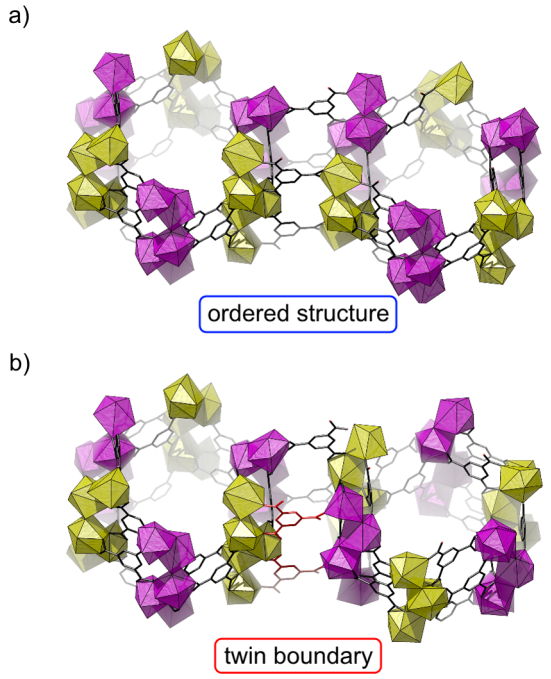

Figure 8. Twinning in CAU-17. Right-handed and left-handed rods are colored purple and yellow, respectively. (a) Two hexagonal channels connected by a RRLL rectangle within an ordered domain as outlined in blue in Figure 7a. (b) Twinning causes some rods across the twin boundary to change in handedness, and the RRLL rectangle between two hexagonal channels is converted into a RLRL channel as outlined in red in Figure 7a. A BTC^{3-} ligand shifted due to twinning is colored red and distorts the Bi−O coordination polyhedron.

links one oxygen atom of a carboxylate group is distanced further (3.3 Å) than this typical range (Figure 8b). Rotation of the carboxylate group would bring both oxygen atoms of the carboxylate group within 2.8 Å of the Bi^{3+} ion.

CONCLUSION

A highly complicated porous Bi-MOF was synthesized, and its crystal structure, topology, and twinning have been presented. The MOF is built of helical rods that are connected by organic tritopic linkers resulting in a crystal structure with five crystallographically independent channels. The topology of the inner walls of the two hexagonal channels alone resembles that of achiral carbon nanotubes. The deconstruction of the rods reveals face-sharing octahedra that are a distorted variation of achiral helices. The 3-periodic net of the reported structure is by far the most complicated net we are aware of among MOFs and surprisingly arises from the assembly of simple building units. While the crystallographic complexity of a MOF can in some cases be enhanced through the choice of larger organic linker molecules, the development of topologically complex frameworks with potentially complex functions and properties still remains a challenge.

A detailed examination of the crystal formation of CAU-17 and transformation mechanisms studied by *in situ* X-ray powder diffraction during solvothermal synthesis is the focus of ongoing work, along with experiments on the catalytic activity, sorption properties, thermal stability, chemical stability, and as a drug delivery host. The title compound was synthesized from the inexpensive starting materials H_3BTC, $Bi(NO_3)_3{\cdot}5H_2O$, and methanol under short reaction times. Crystal structures that form under short reactions times are often overlooked as they can transform into other crystalline phases with prolonged reaction time. Thus, we expect further opportunities to discover unique novel framework structures by closely following the early stages of synthesis.

EXPERIMENTAL SECTION

Synthesis of CAU-17. All chemicals were purchased and obtained from Aldrich, Alfa Aesar, or BASF. They were used without further purification. Synthesis was carried out under solvothermal conditions in a Biotage Initiator microwave oven with 10 mL vials. Suitable single crystals were obtained by mixing H_3BTC (62.5 mg, 297 μmol) and ground $Bi(NO_3)_3{\cdot}5H_2O$ (125.5 mg, 259 μmol) with 5 mL of MeOH at room temperature. The sealed glass vial was shaken by hand for 1 min and subsequently heated in the microwave oven to 120 °C for 20 min with 600 rpm stirring. The obtained colorless single crystals were collected by filtration. X-ray powder diffraction was performed to confirm the purity of the sample (Figure S10). The motivation for the synthesis of the title MOF is described in the Supporting Information.

Structure Determination and Topological Analysis. Additional details of the X-ray diffraction experiment, structure determination, and refinement are provided in the Supporting Information. Single-crystal X-ray diffraction data were collected at the Beamline I19, Diamond Light Source, Didcot, UK. However, structure determination was impeded by twinning in all examined crystals. Rotation electron diffraction (RED) was performed to check for any form of nonmerohedral twinning in CAU-17.[41] The structure was solved from the X-ray data using direct methods in SHELXS and refined using a full-matrix least-squares technique on F^2 with SHELXL.[42]

The underlying net of CAU-17 was determined by identifying the points of extension and links through inspection of the crystal structure. Systre[40] was used to determine the symmetry of the underlying net and obtain a preferred (equal edge) embedding. The resulting net was inspected using the TOPOS package.[43] Models of the twin boundary and models of the misalignment of ligands were created in Materials Studio 7.0.[44]

CCDC 1426169 contains the crystallographic data for this paper. The data can be obtained free of charge from The Cambridge Crystallographic Data Centre via http://www.ccdc.cam.ac.uk/getstructures.

Elemental Analysis and Thermogravimetric Analysis. Thermogravimetric analysis (Figure S11) and elemental analysis were performed to determine the content of disordered solvent molecules in the pores. Elemental chemical analysis was performed on a EuroEA elemental analyzer to determine the carbon, hydrogen, and nitrogen contents in CAU-17: observed C 23.92%, H 1.97%, N 0.00%. Calculated values based on the molecular formula $[Bi(BTC)(H_2O)]{\cdot}2H_2O{\cdot}MeOH$: C 23.64%, H 2.61%, N 0.00%. Thermogravimetric analysis (TGA) was performed on a Netzsch STA 409C in air in an aluminum oxide crucible (heating rate 1 °C/min). Two steps between room temperature and 220 °C were attributed to the loss of three water molecules and one solvent methanol molecule per Bi^{3+} cation (calc. 17.14%, obs. 15.56%). At 350 °C a sharp loss is observed corresponding to the decomposition of the linker (calc. 36.46%, obs. 35.39%) resulting in Bi_2O_3.

ASSOCIATED CONTENT

Supporting Information

The Supporting Information is available free of charge on the ACS Publications website at DOI: 10.1021/jacs.5b12484.

XPD, TGA, SEM images, X-ray crystallographic data, synthesis motivation, RED, thermal ellipsoids, and additional structural and topological figures (PDF)

CIF files for CAU-17 (CIF)

Systre file of the net (TXT)

DOI: 10.1021/jacs.5b12484
J. Am. Chem. Soc. 2016, 138, 1970−1976

AUTHOR INFORMATION

Corresponding Authors

*E-mail: andrew.inge@mmk.su.se.
*E-mail: mokeeffe@asu.edu.
*E-mail: stock@ac.uni-kiel.de.

Notes

The authors declare no competing financial interest.

ACKNOWLEDGMENTS

This work has been supported by the DFG (SPP 1415) and MATsynCELL. A.K.I. is supported by the Knut and Alice Wallenberg Foundation (KAW) through the MAX IV postdoctoral scholarship. M.O.K. is supported by the US National Science Foundation grant number 1104798. H. Xu acknowledges the post-doctoral grant from the Wenner-Gren Foundations. We thank KAW for the project grant 3DEM-NATUR and a grant for purchasing the TEMs. We thank Diamond Light Source and the staff of Beamline I19 for the opportunity to collect X-ray diffraction data and particularly Dr. Sarah A. Barnett for the assistance in data processing. We thank Dr. Helge Reinsch and Prof. Junliang Sun for the fruitful discussions. We also thank Bart Bueken for the scanning electron micrographs.

REFERENCES

(1) Konnert, J. H.; Appleman, D. E. *Acta Crystallogr., Sect. B: Struct. Crystallogr. Cryst. Chem.* **1978**, *34*, 391.
(2) Yaghi, O. M.; O'Keeffe, M.; Ockwig, N. W.; Chae, H. K.; Eddaoudi, M.; Kim, J. *Nature* **2003**, *423*, 705.
(3) Furukawa, H.; Cordova, K. E.; O'Keeffe, M.; Yaghi, O. M. *Science* **2013**, *341*, 1230444.
(4) Allendorf, M. D.; Stavila, V. *CrystEngComm* **2015**, *17*, 229.
(5) Cheetham, A. K.; Rao, C.; Feller, R. K. *Chem. Commun.* **2006**, 4780.
(6) Czaja, A. U.; Trukhan, N.; Müller, U. *Chem. Soc. Rev.* **2009**, *38*, 1284.
(7) Kreno, L. E.; Leong, K.; Farha, O. K.; Allendorf, M.; Van Duyne, R. P.; Hupp, J. T. *Chem. Rev.* **2012**, *112*, 1105.
(8) Murray, L. J.; Dincă, M.; Long, J. R. *Chem. Soc. Rev.* **2009**, *38*, 1294.
(9) Li, M.; Li, D.; O'Keeffe, M.; Yaghi, O. M. *Chem. Rev.* **2014**, *114*, 1343.
(10) Yaghi, O. M.; Li, H.; Eddaoudi, M.; O'Keeffe, M. *Nature* **1999**, *402*, 276.
(11) Chui, S. S.-Y.; Lo, S. M.-F.; Charmant, J. P.; Orpen, A. G.; Williams, I. D. *Science* **1999**, *283*, 1148.
(12) Férey, G.; Serre, C.; Mellot-Draznieks, C.; Millange, F.; Surblé, S.; Dutour, J.; Margiolaki, I. *Angew. Chem.* **2004**, *116*, 6456.
(13) O'Keeffe, M. *Mater. Res. Bull.* **2006**, *41*, 911.
(14) Wang, B.; Côté, A. P.; Furukawa, H.; O'Keeffe, M.; Yaghi, O. M. *Nature* **2008**, *453*, 207.
(15) Hafizovic, J.; Bjørgen, M.; Olsbye, U.; Dietzel, P. D.; Bordiga, S.; Prestipino, C.; Lamberti, C.; Lillerud, K. P. *J. Am. Chem. Soc.* **2007**, *129*, 3612.
(16) Furukawa, H.; Ko, N.; Go, Y. B.; Aratani, N.; Choi, S. B.; Choi, E.; Yazaydin, A. Ö.; Snurr, R. Q.; O'Keeffe, M.; Kim, J.; et al. *Science* **2010**, *329*, 424.
(17) Maji, T. K.; Matsuda, R.; Kitagawa, S. *Nat. Mater.* **2007**, *6*, 142.
(18) Rosi, N. L.; Kim, J.; Eddaoudi, M.; Chen, B.; O'Keeffe, M.; Yaghi, O. M. *J. Am. Chem. Soc.* **2005**, *127*, 1504.
(19) He, Y.; Xiang, S.; Zhang, Z.; Xiong, S.; Fronczek, F. R.; Krishna, R.; O'Keeffe, M.; Chen, B. *Chem. Commun.* **2012**, *48*, 10856.
(20) O'Keeffe, M.; Yaghi, O. M. *Chem. Rev.* **2012**, *112*, 675.
(21) Song, B.-Q.; Wang, X.-L.; Zhang, Y.-T.; Wu, X.-S.; Liu, H.-S.; Shao, K.-Z.; Su, Z.-M. *Chem. Commun.* **2015**, *51*, 9515.
(22) Li, M.; Li, D.; O'Keeffe, M.; Su, Z.-M. *Chem. Commun.* **2015**, *51*, 12228.
(23) Burrows, A. D.; Jurcic, M.; Mahon, M. F.; Pierrat, S.; Roffe, G. W.; Windle, H. J.; Spencer, J. *Dalton Trans.* **2015**, *44*, 13814.
(24) Keogan, D. M.; Griffith, D. M. *Molecules* **2014**, *19*, 15258.
(25) Sun, H.; Zhang, L.; Szeto, K.-Y. In *Met. Ions Biol. Syst.*; Sigel, A., Sigel, H., Eds.; FontisMedia S.A. and Marcel Dekker, Inc.: Lausanne, 2004; Vol. *41*, p 333.
(26) Tiekink, E. R. *Critical reviews in oncology/hematology* **2002**, *42*, 217.
(27) Feyand, M.; Köppen, M.; Friedrichs, G.; Stock, N. *Chem. - Eur. J.* **2013**, *19*, 12537.
(28) Sushrutha, S.; Natarajan, S. *Cryst. Growth Des.* **2013**, *13*, 1743.
(29) Wibowo, A. C.; Smith, M. D.; zur Loye, H.-C. *CrystEngComm* **2011**, *13*, 426.
(30) Wibowo, A. C.; Smith, M. D.; zur Loye, H.-C. *Chem. Commun.* **2011**, *47*, 7371.
(31) Wang, G.; Liu, Y.; Huang, B.; Qin, X.; Zhang, X.; Dai, Y. *Dalton Trans.* **2015**, *44*, 16238.
(32) Feyand, M.; Mugnaioli, E.; Vermoortele, F.; Bueken, B.; Dieterich, J. M.; Reimer, T.; Kolb, U.; De Vos, D.; Stock, N. *Angew. Chem., Int. Ed.* **2012**, *51*, 10373.
(33) Savage, M.; Yang, S.; Suyetin, M.; Bichoutskaia, E.; Lewis, W.; Blake, A. J.; Barnett, S. A.; Schröder, M. *Chem. - Eur. J.* **2014**, *20*, 8024.
(34) Reinsch, H.; van der Veen, M. A.; Gil, B.; Marszalek, B.; Verbiest, T.; De Vos, D.; Stock, N. *Chem. Mater.* **2013**, *25*, 17.
(35) Millange, F.; Serre, C.; Férey, G. *Chem. Commun.* **2002**, 822.
(36) Barthelet, K.; Marrot, J.; Férey, G.; Riou, D. *Chem. Commun.* **2004**, 520.
(37) Wilder, J. W.; Venema, L. C.; Rinzler, A. G.; Smalley, R. E.; Dekker, C. *Nature* **1998**, *391*, 59.
(38) Janiak, C. *J. Chem. Soc., Dalton Trans.* **2000**, 3885.
(39) Lidin, S.; Andersson, S. *Z. Anorg. Allg. Chem.* **1996**, *622*, 164.
(40) Delgado-Friedrichs, O.; O'Keeffe, M. *Acta Crystallogr., Sect. A: Found. Crystallogr.* **2003**, *59*, 351.
(41) Wan, W.; Sun, J.; Su, J.; Hovmöller, S.; Zou, X. *J. Appl. Crystallogr.* **2013**, *46*, 1863.
(42) Sheldrick, G. *Acta Crystallogr., Sect. A: Found. Crystallogr.* **2008**, *64*, 112.
(43) Blatov, V.; Shevchenko, A.; Serezhkin, V. *J. Appl. Crystallogr.* **2000**, *33*, 1193.
(44) *Materials Studio*, 7.0 ed.; Accelrys Software Inc.: San Diego, CA, 2013.

DOI: 10.1021/jacs.5b12484
J. Am. Chem. Soc. 2016, 138, 1970−1976